On the Solution of Equilibrium Points of Power Systems With Penetration of Power Electronics Considering Converter Limitation

Jie Song, Marc Cheah-Mane, *Member, IEEE,* Eduardo Prieto-Araujo, *Member, IEEE,* and Oriol Gomis-Bellmunt, *Fellow, IEEE*

Abstract—Increasing penetration of power electronics is changing the understanding of modern power systems. In particular, current saturation of converters might lead to multiple equilibrium points for both normal and short-circuit conditions. This paper aims to identify multiple equilibrium points in power systems with penetration of power electronics. First, a steady-state model of power systems considering the power electronics operation is presented. Then, a general methodology is developed to obtain equilibrium points including all possible combinations of converter current saturation states. A system of equations is defined for each combination and is solved considering the possibility to have single or multiple solutions. This methodology is suitable for steady-state analysis in normal operation and during short-circuit scenarios. Test systems with Voltage Source Converters are used to validate the presented methodology.

Index Terms—Steady-state analysis, current saturation, voltage source converter, short-circuit calculation, operation limits.

I. INTRODUCTION

MODERN power systems have been increasingly penetrated with power electronics at different levels. This can be explained with the rapid growth of renewable energy generation, transport electrification, industrial electric-drives, deployment of batteries in power systems, flexible AC transmission system (FACTS) and high-voltage direct current (HVDC) transmission [1]. Non-linear operation characteristics introduced with the penetration of power electronics are significantly changing the understanding of power systems [2]. In particular, the converter control modes should be considered when analyzing the equilibrium operation points in a power system. Besides, compared to conventional components, converter control saturates current in case of overload or faults. Such current saturation represents a different converter operation that should be considered in steady-state analysis for both normal and short-circuit conditions. As a result, power systems with large number of power converters might have multiple equilibrium operation points depending on the converters that reach current saturation. In other words, multiple

The authors are with the Centre d'Innovació Tecnològica en Convertidors Estàtics i Accionaments, Departament d'Enginyeria Elèctrica, Universitat Politècnica de Catalunya, Barcelona 08028, Spain (E-mails: jie.song,marc.cheah,eduardo.prieto-araujo,oriol.gomis@upc.edu). Marc Cheah-Mane and Eduardo Prieto-Araujo are also Serra Húnter Lecturers. Oriol Gomis-Bellmunt is also an ICREA Academia researcher.

equilibrium points can be obtained, where different converters are unsaturated or saturated. This is especially critical for short-circuit calculations where several (or all) converters might be saturating current.

Short-circuit analysis of power electronics dominated power systems has been addressed in the literature. A comprehensive study on short-circuit characteristic of VSC based DC network is presented in [3] considering different distributed generation sources. A control strategy of Modular Multilevel Converter (MMC) during DC faults is presented in [4]. Short-circuit current of MMC during AC faults is obtained using a discrete-time model in [5]. These references are based on dynamic simulations and are mainly focused on the converter response. While the previous studies provide interesting insights, the proposed methodology cannot identify solutions for all combinations of converter states and therefore it can provide limited information. Furthermore, it requires to run specific simulations case by case. This can be addressed using a steady-state approach (as suggested in this paper) which is common in analysis of conventional power systems.

Steady-state analysis of power systems including power electronics has also been widely reported in the literature. A sequential AC/DC power flow calculation is presented in [6] considering converter control modes and current limitation. Also, Optimum Power Flow (OPF) algorithms considering a meshed AC/DC grid are presented in [7], [8]. Although VSC operation limits are included in previous references, short-circuit conditions and multiple solutions related to different converter current saturation states have not been considered.

On the other hand, the existence of multiple equilibrium points and the non-uniqueness of solutions in traditional power systems has been discussed in the literature. Conditions for the existence of multiple power flow solutions were derived in [9]. The number of power flow solutions in small-scale power systems is obtained based on the power and voltage level in [10]. An explicit condition that guarantees the existence and uniqueness of the load-flow solution for distribution networks is presented in [11]. A sufficient conditions for multiple power flow solutions existence has been derived in three-phase unbalanced systems [12]. However, the possibility to have multiple solutions with power electronics differs from the classic problems analyzed in [9]–[12], since they are highly dependent on the non-linear characteristic of the converters when current is saturated. Moreover, in normal operation, the system usually attempts to operate in an equilibrium

point with the highest voltage level [13]. Nevertheless, the identification of all equilibrium points might be necessary in some power systems studies, such as estimation of voltage instability margin [14] or short-circuit analysis.

In this direction, methodologies to obtain multiple equilibrium points have been explored for conventional power systems. Many efforts have been put into the identification of multiple equilibrium points in small-scale DC systems [15]–[17]. A numerical continuation methodology that claims to find all power flow solutions in AC grids is presented in [18]. This algorithm traces a smooth curve starting from a known solution to locate all the other solutions. Such methodology has been revised in [19] to connect additional complex solutions. The Numerical Polynomial Homotopy Continuation (NPHC) method has been employed to trace all solutions from power systems equations [13]. However, the operation of power electronics is not included in the literature to the best of authors' knowledge.

This paper presents a methodology for steady-state analysis of power systems with power electronics elements. In particular, the paper contributions are as follows:

- A generic steady-state formulation of power systems equations including the power electronics operation in different control modes and current saturation states.
- A methodology to identify equilibrium points of the power systems in including all combinations of converter current saturation states. This methodology is suitable for steady-state analysis of power systems in both normal operation and short-circuit conditions.

The existence of multiple solutions is considered for each combination of converter current saturation states. In particular, two options to solve the system of equations are presented depending on the possibility to have single or multiple solutions. Power systems presented in this paper are analyzed under balanced three-phase conditions and are expressed in single-phase using per-unit values. The presented methodology for steady-state analysis is validated with examples of power systems including VSCs in different control modes.

II. EQUIVALENT MODEL OF VSC

A. Steady-state modeling of VSC operation

The VSC equivalent model is presented in this Section, as it is an essential component defining the system of equations for power systems with penetration of power electronics. The equivalent scheme of a VSC connected to an AC grid is shown in Fig. 1, where the VSC equivalent model is represented with a voltage source, $\underline{u}_{vsc}$, and a phase reactor, $\underline{z}_{vsc}$.

The VSC is connected to the AC grid at the Converter Connection Point (CCP) [20], where the power exchange between the VSC and the AC grid is regulated by the VSC and can be expressed as follows:

$$p + jq = \underline{u}_{con}\underline{i}_{vsc}^*\qquad(1)$$

where p and q are the active and reactive power exchanged with the grid, $\underline{u}_{con}$ is the voltage at the CCP and $\underline{i}_{vsc}$ is the
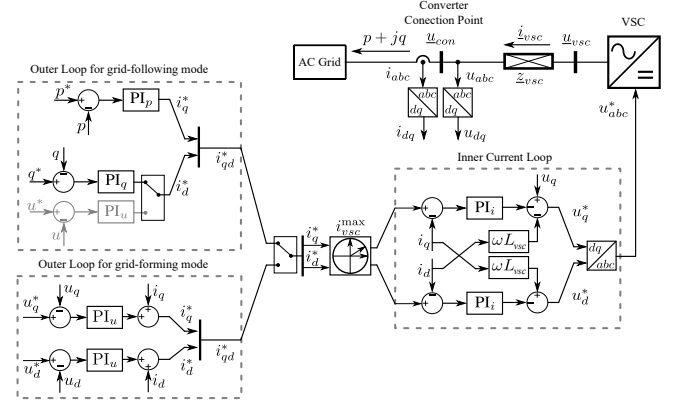

Fig. 1. VSC equivalent diagram and the control loop scheme

current injected into the grid. Then, the converter voltage $\underline{u}_{vsc}$ can be obtained as:

$$\underline{u}_{vsc} = \underline{u}_{con} + \underline{i}_{vsc}\underline{z}_{vsc}\qquad(2)$$

Additional characterizing equations are included considering different VSC control modes. The VSC in grid-following mode (in particular PQ, PV and grid-support (GS) controls) and grid-forming (GF) mode are presented in this paper. As a result, the VSC equivalent model includes the following constraints for each control mode:

$$\begin{cases} p = p_{ref};\ q = q_{ref} & \text{if PQ mode} \\ p = p_{ref};\ u_{con} = u_{ref} & \text{if PV mode} \\ p = p_{ref};\ q = q_{ref} + u_{con}k_{isp}(u_{ref} - u_{con}) & \text{if GS mode} \\ u_{con} = u_{ref};\ \theta_{\underline{u}_{con}} = \theta_{ref} & \text{if GF mode} \end{cases}$$
$$(3)$$

where p_{ref} and q_{ref} are the active and reactive power reference, u_{ref} is the AC voltage magnitude reference, k_{isp} is the voltage droop gain for grid-support as reactive current and θ_{ref} is the angular reference of $\underline{u}_{con}$ in grid-forming mode. Reactive power injection from VSC in GS mode consists of both a constant value, q_{ref}, and a voltage droop characteristic, $u_{con}k_{isp}(u_{ref} - u_{con})$. Dead-bands of reactive current for grid-support modes are applied in some applications. But they are not included in this paper for the sake of simplicity.

These VSC control modes are represented in Fig. 1 as the outer loops. In case of VSC in PV mode, the reactive power control is replaced with an AC voltage control [21]. In case of VSC in grid-forming mode, the outer loop is replaced with a voltage control loop implemented in qd frame [22]. The inner control loop, also implemented in qd frame with i_q corresponding to active power and i_d to reactive power, tracks the current reference generated by the outer loop.

Current saturation must also be implemented into the VSC control loop in order to protect the converter from overloading as shown in Fig. 1. In particular, the current reference magnitudes will be saturated at specific value i_{vsc}^{max}. Anti-windup schemes are typically employed, but they also are not shown in Fig. 1 for the sake of simplicity. VSC operation can be divided into three states considering the current saturation:

- *Unsaturated state (USS)*: current limitation is not reached. VSC follows the reference values as presented in (3).

3

- *Partially saturated state (PSS)*: the total current from VSC is saturated at the nominal value and the power or voltage reference defined in (3) cannot be achieved. This state is not applied to grid-forming VSCs as they are not controlling active power directly. Usually, active power component is reduced to prioritize the reactive power component for grid-following VSCs [23], which defines the following constraints:

$$\begin{cases} i_{vsc} = i_{vsc}^{\max}; \ q = q_{ref} & \text{if PQ mode} \\ i_{vsc} = i_{vsc}^{\max}; \ u_{con} = u_{ref} & \text{if PV mode} \\ \begin{cases} i_{vsc} = i_{vsc}^{\max} \\ q = q_{ref} + k_{isp}u_{con}(u_{ref} - u_{con}) \end{cases} & \text{if GS mode} \end{cases} \quad (4)$$

where $i_{vsc}^{\max}$ is the VSC nominal current. However, active power could be prioritized with similar formulations.

- *Fully saturated state (FSS)*: the total current from VSC is saturated and both active and reactive power are limited. In this case, active power is set to 0 in order to prioritize reactive power [23] for grid-following VSCs. The grid-forming VSC, instead of holding a constant voltage, maintains the current magnitude at the nominal value and following the reference current angle, $\angle\theta_i^{ref}$, for FSS. Therefore, the following constraints are defined:

$$\begin{cases} i_{vsc} = i_{vsc}^{\max}; \ p = 0 & \text{if PQ/PV/GS mode} \\ \underline{i}_{vsc} = i_{vsc}^{\max}\angle\theta_i^{ref} & \text{if GF mode} \end{cases} \quad (5)$$

B. Operation limits of VSC

The identified equilibrium points of the power system should satisfy the operation limits for all VSCs in the system. The typical conditions to be checked for validation of all possible solutions are expressed as follows:

$$\begin{cases} i_{vsc} \le i_{vsc}^{\max} \\ u_{vsc} \le u_{vsc}^{\max} \\ p_{\min} \le p_{vsc} \le p_{\max} \\ q_{\min} \le q_{vsc} \le q_{\max} \end{cases} \quad (6)$$

The current limitation in (6) is a critical condition to be checked for the solutions obtained when VSC is operating in USS. However, the solutions obtained with VSC in PSS or FSS, compared to USS, naturally satisfy the current limitation as the current constraint $i_{vsc} = i_{vsc}^{\max}$ is included in the system of equations as presented in (4) and (5).

Voltage magnitude is also limited by the capability of VSCs in (6). Upper limits will be set for the magnitude of converter voltage, u_{vsc}, to avoid over-modulation of switching bridges. Besides, active and reactive power injection from each VSC should be regulated within corresponding upper and lower limits at the CCP as expressed in (6). Usually, the upper and lower bound of active and reactive powers are defined by the operation limits of the element or the grid connected with the studied system through a VSC. For example, PV plants cannot inject active power higher than the available power or receive active power from the grid [23]. Thus, the active power upper limit of of the VSC is set at the maximum available value, *i.e.* $p_{\max} = p_{nom}$, while the lower limit is set at 0, *i.e.* $p_{min} = 0$.

III. STEADY-STATE MODELING OF POWER SYSTEMS WITH POWER ELECTRONICS

A general steady-state formulation for power systems with power electronics is presented in this Section. The circuit of a power system can be defined with the admittance matrix, $\mathbf{Y}$, which is expressed as follows:

$$\begin{bmatrix} \underline{i}_1 \\ \vdots \\ \underline{i}_A \end{bmatrix} = \underbrace{\begin{bmatrix} \underline{y}_{11} & \cdots & \underline{y}_{1A} \\ \vdots & \ddots & \vdots \\ \underline{y}_{A1} & \cdots & \underline{y}_{AA} \end{bmatrix}}_{\mathbf{Y}} \begin{bmatrix} \underline{u}_1 \\ \vdots \\ \underline{u}_A \end{bmatrix} \quad (7)$$

where A is the number of total buses in the studied system, $\underline{u}_a$ is the voltage at bus a for $a \in [1, A]$ and $\underline{i}_a$ is the current injection at bus a. The impedances from power electronics and non-power electronics elements connected to each bus are excluded from the $\mathbf{Y}$ matrix since the current injection from these elements is considered in $\underline{i}_a$, which is expressed as:

$$\underline{i}_a = \sum\nolimits_{m=1}^{M_a} \underline{i}_{a,m} \ \forall a \in [1, A] \quad (8)$$

where M_a is the number of elements connected to bus a and $\underline{i}_{a,m}$ is the current injection from element m at bus a for $m \in [1, M_a]$. In the case where no element is connected to bus a, the current injection is defined as $\underline{i}_a = 0$.

The current injection $\underline{i}_{a,m}$ is defined in a set of constraints H (see (9)) that corresponds to the equivalent model of each element. Non-power electronics elements usually operate in the same state without being saturated. Thus, the expression of current injection from these elements will not be modified. However, power electronics elements can operate in different current saturation states, which results in different equations within constraints H to present the power system under study. In case of VSCs, the expressions of power electronics operation in the constraints follows the equivalent model presented in Section II. Since solutions may exist in a system of equations corresponding to any combination of the power electronics current saturation states, all possible combinations should be included in constraints H.

If the system under study contains a total number of N power electronics elements, while the number of current saturation states in each element n, for $n \in [1, N]$, is denominated by x_n, then the number of all possible combinations of power electronics current saturation states, F, can be expressed as: $F = \prod_{n=1}^{N} x_n$. As a result, the set of current injection constraints H contains F subsets of equations, that represent each combination, such that:

$$H = \begin{bmatrix} H_1 & \cdots & H_f & \cdots & H_F \end{bmatrix}^T \quad (9)$$

where H_f, for $f \in [1, F]$, is the subset of equations defining current injection from both power electronics and non-power electronics elements for combination f. The constraints H_f can be expressed as:

$$H_f = \begin{bmatrix} h_{1-f} & \cdots & h_{m-f} & \cdots & h_{M-f} \end{bmatrix}^T \quad (10)$$

where M is the number of elements contained in the studied system and h_{m-f} is the set of equations defining current

injection from element m operating in combination f for $m \in [1, M]$.

In some cases, current injection from element m, can be expressed in an explicit form as follows:

$$\begin{cases} h_{m-f} := \underline{i}_{a,m} = \underline{i}_{ref,m} & \text{if current source} \\ h_{m-f} := \underline{i}_{a,m} = \dfrac{\underline{u}_{th,m} - \underline{u}_k}{\underline{z}_{th,m}} & \text{if Thévenin eq.} \\ h_{m-f} := \underline{i}_{a,m} = \left(\dfrac{p_{ref,m} + j q_{ref,m}}{\underline{u}_k} \right)^* & \text{if PQ node} \end{cases}$$
$$(11)$$

where $\underline{i}_{ref,m}$ is the reference of a current source, $\underline{u}_{th,m}$ and $\underline{z}_{th,m}$ are the Thévenin equivalent voltage and impedance respectively, $p_{ref,m}$ and $q_{ref,m}$ are active and reactive power reference for a PQ node. In other cases, current injection cannot be presented in an explicit form. Therefore, it is expressed by implicit equations in constraints H. The definition of a PV node is used as an example as follows:

$$h_{m-f} := \begin{bmatrix} u_a = u_{ref} \\ \text{Re}\left(\underline{u}_a \underline{i}_{a,m}^* \right) = p_{ref} \end{bmatrix} \text{ if PV node} \qquad (12)$$

where u_{ref} is the voltage reference and p_{ref} is the active power reference for a PV node. Current saturation states corresponding to PSS and FSS can be also expressed in a similar format from equations in (4) and (5).

The admittance matrix in the system of equations is the same for all combinations, while for each combination, a subset of equations H_f will be selected defining current injections. Then, the system of equations, SE_f, corresponding to a combination $f \in [1, F]$, can be expressed as follows combining (7), (8) and (10):

$$SE_f := \begin{cases} \begin{bmatrix} \underline{i}_{1-f} \\ \vdots \\ \underline{i}_{A-f} \end{bmatrix} = \underbrace{\begin{bmatrix} \underline{y}_{11} & \cdots & \underline{y}_{1A} \\ \vdots & \ddots & \vdots \\ \underline{y}_{A1} & \cdots & \underline{y}_{AA} \end{bmatrix}}_{\mathbf{Y}} \begin{bmatrix} \underline{u}_{1-f} \\ \vdots \\ \underline{u}_{A-f} \end{bmatrix} \\ \underline{i}_{a-f} = \sum_{m=1}^{M_a} \underline{i}_{a,m-f} \; \forall a \in [1, A] \\ H_f = \begin{bmatrix} h_{1-f} & \cdots & h_{m-f} & \cdots & h_{M-f} \end{bmatrix}^T \end{cases}$$
$$(13)$$

This formulation presents a flexible structure to represent power systems with penetration of power electronics considering different operation modes and also the possibility to include converter current saturation. Therefore, this is suitable for steady-state analysis in both normal operation and short-circuit conditions.

IV. IDENTIFICATION OF POWER SYSTEMS EQUILIBRIUM POINTS

Equilibrium points in a power system may exist for each combination of converter current saturation states. The systems of equations SE_f, as defined in (13), represent each combination $f \in [1, F]$. Such system of equations must be solved in order to identify equilibrium points for all possible converter current saturation states. Also, multiple solutions may be obtained from each system of equations corresponding to a combination f. Therefore, two options regarding the solutions number for each combination are defined as follows:

- *Single-Solution (SS)*: this option returns one equilibrium point for each combination. In this case, systems of equations are solved using an iterative method, *e.g.* Newton-Raphson method, where the definition of initial conditions is essential to find specific solutions.
- *Multiple-Solutions (MS)*: this option identifies all possible equilibrium points for each combination. The NPHC method has been employed in this paper to solve power system equations in MS option. This method is implemented through the mathematical software, *PHCpack*, which requests the system of equations defined in (13) as the input and returns all solutions for each combination [24]. However, the NPHC method usually require higher computation compared to iterative methods adopted in SS option [25].

The methodology to identify equilibrium points of power systems with penetration of power electronics is summarized as shown in Algorithm 1. The two previously-defined options regarding the solutions number for each combination are considered. Admittance matrix of the circuit, $\mathbf{Y}$, current injection constraints, H, operation limits of VSCs in (6) and the selected option, opt, are defined as the input information of the algorithm.

The system of equations SE_f is defined based on the admittance matrix of the circuit, $\mathbf{Y}$, and the current injection constraints, H_f, associated for each combination $f \in [1, F]$. Then, SE_f is solved with single or multiple-solutions based on opt. In SS option, the number of returned equilibrium points is equal to the combinations number of the studied system, F. In MS option, the number of returned solutions can be expressed as: $N_s = \sum_{f=1}^{F} N_{s,f}$, where $N_{s,f}$ is the number of solutions obtained from system of equations SE_f. Finally, the equilibrium points are validated according to the VSCs operation limits as defined in (6). The solutions that violate these limits will be marked as no solution.

V. NUMERICAL TEST AND VALIDATION

The methodology for identification of equilibrium points is implemented and validated in this Section. Results are obtained for three test systems based on VSCs. Test System 1 and 2 employ both the SS and MS option while Test System 3 employs only SS option due to computing time limits.

A. Test System 1

This test system is composed by an AC grid Thévenin equivalent and a VSC in PV mode, while an output impedance $\underline{z}_{out}$ is connected to bus 1 as shown in Fig. 2.

The VSC is the only power electronics element in this test system. As a result, the number of combinations is equal to the number of the VSC's potential current saturation states (USS, PSS and FSS), *i.e.* $F = 3$. Following the general formulation in (13), the system of equations for Test System 1 corresponding to combination f, for $f \in [1, 3]$, is expressed as follows:

$$SE_f := \begin{cases} \underline{i}_{1-f} = \underline{y}_{11} \underline{u}_{out-f} \\ \underline{i}_{1-f} = \underline{i}_{th-f} + \underline{i}_{vsc-f} \\ H_f = \begin{bmatrix} h_{1-f} & h_{2-f} \end{bmatrix}^T \end{cases} \qquad (14)$$

Algorithm 1: Identification of equilibrium points

input : Admittance matrix $\mathbf{Y}$
        Constraints H
        VSCs operation limits
        option opt

output: Identified equilibrium (eq.) points set EP

begin
   $m = 0$; // index of saved eq. points
   for $f \leftarrow 1$ **to** F **do**
      define system of equations SE_f with H_f;
      switch opt **do**
         case SS **do**
            $sol = solve(SE_f); N_{s,f} = 1$;
         end
         case MS **do**
            $sol = NPHCsolve(SE_f)$;
            $N_{s,f} = size(sol)$;
         end
         for $n_{s,f} \leftarrow 1$ **to** $N_{s,f}$ **do**
            if $sol(n_{s,f})$ *satisfies VSCs operation limits*
            then
               $m = m + 1; EP_{(m)} = sol(n_{s,f})$;
            else
               $m = m + 1; EP_{(m)} = no\ solution$;
            end
         end
      end
   end
   return EP; // return all eq. points
end

where the admittance value at bus 1 is defined by the output impedance such that $\underline{y}_{11} = 1/\underline{z}_{out}$. The VSC terminal impedance, $\underline{z}_{vsc}$, and Thévenin equivalent impedance, $\underline{z}_{th}$, are excluded from the admittance following the formulation presented in Section III. The current injection at bus 1 is composed of the Thévenin equivalent current $\underline{i}_{th-f}$, which is defined by h_{1-f}, and VSC current injection $\underline{i}_{vsc-f}$, which is defined by h_{2-f}.
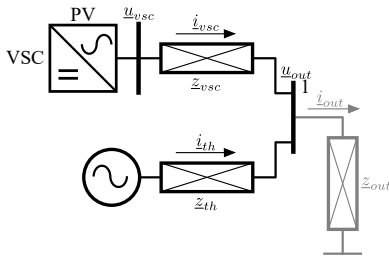

Fig. 2. Scheme of Test System 1

The VSC current injection is modified for each combination of current saturation states (*i.e.* USS, PSS and FSS) based on the implicit equations in constraints H, which follow the VSC equivalent model in PV control as presented in Section II. The Thévenin equivalent current definition is the same for all combinations and is expressed with implicit equations in constraints H. As a result, the current constraints, H_f, can be defined for each state as follows:

$$H_1 = \begin{bmatrix} h_{1-1} := \underline{i}_{th-1} = \left(\underline{u}_{th} - \underline{u}_{out-1}\right)/\underline{z}_{th} \\ h_{2-1} := \begin{bmatrix} \text{Re}\left(\underline{u}_{out-1}\underline{i}_{vsc-1}^*\right) = p_{ref} \\ u_{out-1} = u_{ref} \end{bmatrix} \end{bmatrix} \text{ if USS} \tag{15}$$

$$H_2 = \begin{bmatrix} h_{1-2} := \underline{i}_{th-2} = \left(\underline{u}_{th} - \underline{u}_{out-2}\right)/\underline{z}_{th} \\ h_{2-2} := \begin{bmatrix} i_{vsc-2} = i_{vsc}^{\max} \\ u_{out-2} = u_{ref} \end{bmatrix} \end{bmatrix} \text{ if PSS} \tag{16}$$

$$H_3 = \begin{bmatrix} h_{1-3} := \underline{i}_{th-3} = \left(\underline{u}_{th} - \underline{u}_{out-3}\right)/\underline{z}_{th} \\ h_{2-3} := \begin{bmatrix} \text{Re}\left(\underline{u}_{out-3}\underline{i}_{vsc-3}^*\right) = 0 \\ i_{vsc-3} = i_{vsc}^{\max} \end{bmatrix} \end{bmatrix} \text{ if FSS} \tag{17}$$

The output impedance $\underline{z}_{out}$ has been tested as a resistance with a value increased from 0.05 to 1 pu and a step size of 0.001 pu (951 sampling points in total). All solutions for each inserted output impedance have been obtained following the Algorithm 1 when MS option selected. Then, the system of equations in (14) is solved using the NPHC method and considering the three current injection constraints expressed in (15), (16) and (17), which define each current saturation state combination. Finally, each obtained solution is validated by checking that the VSC operation limits, as expressed in (6), are satisfied, following the values shown in Table VIII (see Appendix).

Fig. 3 shows the converter terminal voltage magnitude u_{vsc}, VSC current magnitude i_{vsc}, and active power injection p_{vsc} corresponding to different output impedances. Also, the gray area represents the range of values for u_{vsc}, i_{vsc} and p_{vsc} where the VSC is out of operation limits. In total, up to six solutions are obtained, two for each VSC current saturation state, which are tagged with the name of the state and a number. It is observed that solution USS-2 is not feasible for all the range of output impedance values since the voltage and current limits are violated. Also, for high output impedances, feasible solutions can be found for all the three combinations, while for low output impedances, solutions only exist for FSS. The VSC in USS always have the same active power injection as expressed in (15). Thus, p_{vsc} curves for USS-1 and USS-2 are overlapped in Fig. 3(c). Similarly, curves of i_{vsc} for PSS and FSS are overlapped in Fig. 3(b) since the VSC follows the same current magnitude when operating in these two states as expressed in (16) and (17).

The calculation is also carried out for SS option sweeping the same output impedances shown in Fig. 3. As a result, one solution is obtained for each VSC current saturation state, which corresponds to the solution curves USS-1, PSS-2 and FSS-1, shown as dashed curves in Fig. 3. Equilibrium points identification in SS option is carried out with MATLAB R2019b while PHCpack 2.4.74 is adopted in MS option. Both software are implemented with a PC with an Intel Core i7-8700k processor and 16GB memory. In MS option, the complete computing process takes 860 s for all the 951
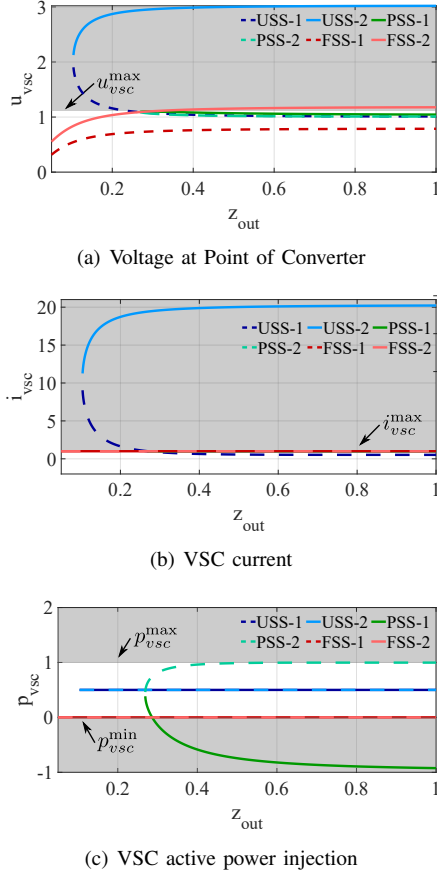
(a) Voltage at Point of Converter

(b) VSC current

(c) VSC active power injection

Fig. 3. Test System 1 solutions curves

TABLE I
SOLUTIONS OF TEST SYSTEM 1

Solution Number	u_{out}	i_{vsc}	p_{vsc}	u_{vsc}	Satisfy VSC operation limits?
$\underline{z}_{out} = 0.8$ pu					
•USS-1	1	0.51	0.5	1.01	✓
USS-2	1	20.18	0.5	3.01	✕
PSS-1	1	1	-0.89	1.05	✕
•PSS-2	1	1	1.00	1.00	✓
•FSS-1	0.89	1	0	0.79	✓
FSS-2	1.07	1	0	1.17	✕
$\underline{z}_{out} = 0.28$ pu					
•• USS-1	1	0.96	0.5	1.08	✓
USS-2	1	19.48	0.5	2.95	✕
PSS-1	1	1	0.087	1.10	✓
•PSS-2	1	1	0.69	1.07	✓
•FSS-1	0.83	1	0	0.73	✓
• FSS-2	1.00	1	0	1.10	✓
$\underline{z}_{out} = 0.08$ pu					
•FSS-1	0.57	1	0	0.47	✓
FSS-2	0.64	1	0	0.74	✓

• solutions obtained in SS option.
• the solution validated with dynamic simulation (slow).
• the solution validated with dynamic simulation (fast).

in Table VIII. As a result, the system shows different equilibrium states in response to the output impedance variation, corresponding to solution USS-1 (marked with • in Table I) and FSS-2 (marked with • in Table I) for $\underline{z}_{out} = 0.28$ pu, which proves the existence of multiple equilibrium points in Test System 1. In particular, with the slow voltage controller, VSC remains in USS, while with the fast voltage controller, VSC hits the current limitation and operates in FSS state.
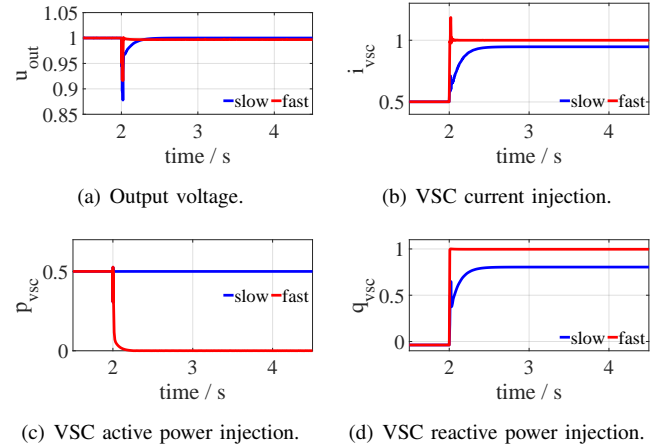

(a) Output voltage.

(b) VSC current injection.

(c) VSC active power injection.

(d) VSC reactive power injection.

Fig. 4. Dynamic validation of Test System 1

B. Test System 2

This test system is a 6-bus mesh grid with the configuration shown in Fig. 5, which is based on the IEEE 9-bus system. Bus 1 is connected to a voltage source that represents the slack bus of the system. Two VSCs are connected to buses 2 and 3, both operating in PQ mode. A load is connected at bus 5 absorbing constant active and reactive power. Transmission cables are characterized as equivalent impedances. The parameters of

different output impedances. As a comparison, the same output impedance range is swept within only 16 s in SS option.

The solutions obtained with different output impedances in MS option are listed in Table I as examples. The solutions that are also obtained in SS option are marked with •. Firstly, the output impedance is defined as a load, such that $\underline{z}_{out} = 0.8$ pu, which represents the system in normal operation. Among all the six obtained solutions, three of them are within the operation limits of the VSC, *i.e.* multiple equilibrium points exist in normal operation. The solutions when $\underline{z}_{out} = 0.28$ pu are also listed as a comparison. Among all the six solutions, five of them are identified as equilibrium points, while solution USS-2 is not valid, since the VSC current and voltage limits are violated. A short-circuit analysis is also carried out by defining a low value output impedance, *e.g.* $\underline{z}_{out} = 0.08$ pu. Then, equilibrium points are only identified when the VSC is operated in FSS, since the solution does not exist in the system of equations with USS and PSS.

Dynamic simulations implemented in MATLAB-Simulink are used to validate the existence of the multiple equilibrium points shown in Table I for $\underline{z}_{out} = 0.28$ pu. The time-domain results of voltage magnitude at bus 1, u_{out}, VSC current magnitude, i_{vsc}, and power injection, p_{vsc} and q_{vsc} are shown in Fig. 4. The output impedance, $\underline{z}_{out}$, is reduced from a large value to 0.28 pu at 2 s, which represents a disturbance for the system. The VSC voltage control has been tested with two different speed responses based on the controller gains listed

Test System 1 are listed in Table VIII. The equilibrium points of this test system are initially obtained in MS option.
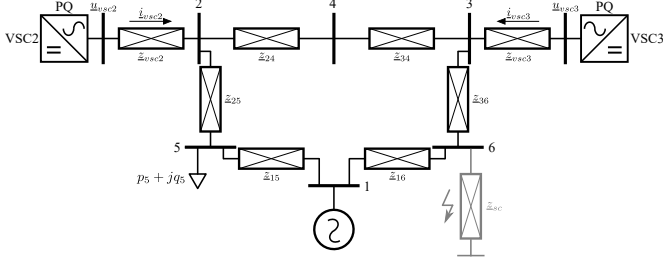

Fig. 5. Scheme of Test System 1

In this case, since three current saturation states (USS, PSS and FSS) are considered in both VSC2 and VSC3, then 9 combinations are defined for this test system, *i.e.* $F = 9$. First, the short-circuit impedance, $\underline{z}_{sc}$, is disconnected from bus 6 for equilibrium points identification in normal operation.

In total 58 solutions are obtained in MS option, but only 21 of them are validated as equilibrium points that satisfy the operation limits of both VSC2 and VSC3, as summarized in Table II. Three of the obtained equilibrium points in normal operation for this studied system are shown in Table III as examples.

It is observed that operation with both VSCs in USS (EP. 1 in Table III) represents a preferred equilibrium point in normal operation, since all VSC references are achieved. However, transient events, such as the example in Fig. 4, can lead to permanent current saturation of specific VSCs, which represent alternative equilibrium points that must be considered.

Then, a short-circuit calculation is carried out by inserting a short-circuit impedance, $\underline{z}_{out} = j0.01$ pu, at bus 6. As a result, 15 among a total of 43 possible solutions are identified as equilibrium points, as shown in Table IV. Compared to normal operation, the system has decreased number of both equilibrium points and total solutions in short-circuit. Three of the obtained equilibrium points in short circuit are listed in Table V as examples.

In this case of short-circuit, there is not a clear equilibrium point as in normal operation. Equilibrium points for combinations where both VSC2 and VSC3 are fully-saturated are more likely to be achieved. This is observed from Table IV, where the number of equilibrium points when both VSCs are operated in FSS is 8 over a total number of 15. Also, it can be noted that no equilibrium points with VSC2 or VSC3 in USS is found.

The calculation for normal operation and short-circuit conditions is repeated in SS option. It is clear that the SS option presents a significant advantage in computing efficiency over MS option as shown in Table VI. Also, in both SS and MS option, the short-circuit calculation takes longer time compared to normal operation equilibrium points identification.

C. Test System 3

This test system is based on the IEEE 30-bus benchmark system with the scheme shown in Fig. 6. A grid-forming VSC is connected at bus 1, which represents the slack bus

TABLE II
NUMBER OF EQUILIBRIUM POINTS/TOTAL SOLUTIONS OF TEST SYSTEM 2 IN NORMAL OPERATION

VSC3 state / VSC2 state	USS	PSS	FSS
USS	1/4	1/4	2/4
PSS	1/6	1/8	2/8
FSS	3/8	3/8	7/8

TABLE III
EQUILIBRIUM POINTS (EP.) EXAMPLES OF TEST SYSTEM 2 IN NORMAL OPERATION

Parameters	EP. 1	EP. 2	EP.3
VSC2 state	USS	FSS	FSS
VSC3 state	USS	USS	FSS
i_{vsc2}	0.42	0.6	0.6
p_{vsc2}	0.41	0	0
q_{vsc2}	0.01	0.54	0.57
i_{vsc3}	0.22	0.23	0.5
p_{vsc3}	0.21	0.21	0
q_{vsc3}	−0.03	−0.03	−0.51
$\underline{u}_2$	$0.97\angle -6.19°$	$0.89\angle -1.72°$	$0.94\angle -1.02°$
$\underline{u}_3$	$0.97\angle -5.17°$	$0.90\angle -2.44°$	$0.94\angle -1.11°$
$\underline{u}_4$	$0.97\angle -5.80°$	$0.91\angle -1.97°$	$0.97\angle -1.05°$
$\underline{u}_5$	$0.98\angle -3.30°$	$0.95\angle -2.10°$	$0.97\angle -1.84°$
$\underline{u}_6$	$0.99\angle -1.75°$	$0.98\angle -0.84°$	$1.00\angle -0.35°$

TABLE IV
NUMBER OF EQUILIBRIUM POINTS/TOTAL SOLUTIONS OF TEST SYSTEM 2 IN SHORT-CIRCUIT ($\underline{z}_{sc} = j0.01$)

VSC3 state / VSC2 state	USS	PSS	FSS
USS	0/3	0/4	0/4
PSS	0/4	1/4	2/4
FSS	0/4	4/8	8/8

of the system when the VSC is operating in USS. In case of FSS, this VSC is operating as a current source. A VSC operated in PQ mode replaces the generator connected at bus 2 in the original system. The VSCs parameters are shown in Table VIII (see Appendix). VSC1 has two potential current saturation states (USS and FSS) while VSC2 can operate in all the three possible states (USS, PSS and FSS) following the VSC equivalent model expressed in Section II. As a result, 6 combinations, *i.e.* $F = 2 \times 3$, are defined for this test system. The transmission lines and transformers are modeled with their equivalent impedance with the parameters from [26].

The system of equations corresponding to each combination is solved in SS option, since the size of the system is too large to be solved as MS within a feasible simulation time. Then, 6 solutions are identified and all of them are validated as equilibrium points of the system that satisfy the VSCs operation limits. The computation time of these 6 equilibrium points in SS option is equal to 2.8 s. Three of the obtained equilibrium points are listed in Table. VII as examples. It can be observed that EP. 1, which is corresponding to both VSCs operating in USS, represents the operation point with the highest voltage level of bus 1 and bus 2. Therefore, this equilibrium point is more likely to be achieved in a normal

TABLE V
EQUILIBRIUM POINT (EP.) EXAMPLES OF TEST SYSTEM 2 IN
SHORT-CIRCUIT ($z_{sc} = j0.01$)

Parameters	EP. 1	EP. 2	EP.3
VSC2 state	PSS	FSS	FSS
VSC3 state	FSS	PSS	FSS
i_{vsc2}	0.6	0.6	0.6
p_{vsc2}	0.38	0	0
q_{vsc2}	0.01	-0.42	-0.44
i_{vsc3}	0.5	0.5	0.5
p_{vsc3}	0	0.21	0
q_{vsc3}	-0.21	-0.03	-0.24
$\underline{u}_2$	$0.63\angle-9.77°$	$0.70\angle-6.17°$	$0.74\angle-3.56°$
$\underline{u}_3$	$0.63\angle-6.96°$	$0.70\angle-7.19°$	$0.74\angle-3.21°$
$\underline{u}_4$	$0.56\angle-9.77°$	$0.59\angle-7.51°$	$0.65\angle-3.78°$
$\underline{u}_5$	$0.87\angle-4.15°$	$0.89\angle-3.37°$	$0.91\angle-2.74°$
$\underline{u}_6$	$0.11\angle7.42°$	$0.11\angle7.13°$	$0.12\angle8.35°$

TABLE VI
COMPUTING TIME OF TEST SYSTEM 2 IN SS AND MS OPTIONS

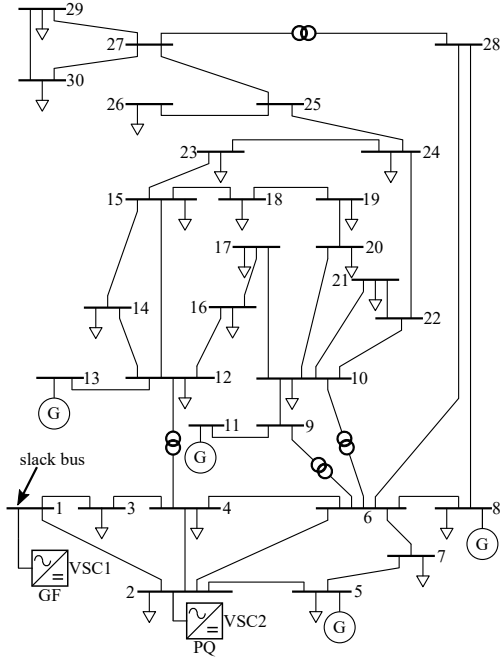| Option \ System States	Normal Operation	Short-Circuit
SS	$0.18\ s$	$0.70\ s$
MS	$2.40\ h$	$13.67\ h$

Fig. 6. Scheme of Test System 3

operation scenario.

VI. CONCLUSION

Steady-state analysis of power systems with penetration of power electronics presents potential multiple equilibrium operation points that differ from classic problems analyzed in the literature. Such multiple equilibrium points are achieved mainly due to the converter current saturation and are specially important in large systems with several converters.

TABLE VII
EQUILIBRIUM POINT (EP.) EXAMPLES OF TEST SYSTEM 3

Parameters	EP. 1	EP. 2	EP.3
VSC1 state	USS	FSS	FSS
VSC2 state	USS	USS	FSS
i_{vsc1}	1.32	1.5	1.5
p_{vsc1}	0.77	1.49	1.30
q_{vsc1}	1.16	0.28	0.29
i_{vsc2}	0.64	0.66	0.75
p_{vsc2}	0.4	0.4	0
q_{vsc2}	0.5	0.5	0.64
$\underline{u}_1$	$1.06\angle0°$	$1.01\angle10.79°$	$0.89\angle12.79°$
$\underline{u}_2$	$1.00\angle-0.97°$	$0.98\angle7.39°$	$0.85\angle9.23°$

This paper has proposed a general steady-state formulation to define systems of equations that include the combinations of converter saturation states. Then, a methodology has been presented to identify multiple equilibrium points for all possible current saturation states of power electronics. In addition, methods to obtain single or multiple solutions for each combination of converter current saturation states are considered. Both approaches result in multiple equilibrium points, as validated in several test systems. In general, single solutions obtained from iterative methods would be selected as preferred option for large power systems due to computation time constraints of multiple-solution options. However, multiple solutions are still useful for specific conditions with a limited number of current saturation combinations.

The presented methodology is suitable for the analysis of power systems in both normal operation and short-circuit conditions, as all potential converter current saturation states are considered. A number of studies can be carried out based on the identified equilibrium points. For example, short-circuit calculation following the presented methodology may lead to multiple equilibrium points that could affect the current protection design of power systems. The identified equilibrium points also provide initialization conditions for small-signal stability analyses and dynamic studies. Further studies can be carried out including different system formulations, *e.g.* with asymmetrical AC grids or hybrid AC-DC systems.

APPENDIX

Table VIII includes the parameters of all the case studies shown in Section V.

REFERENCES

[1] X. Wang and F. Blaabjerg, "Harmonic stability in power electronic-based power systems: Concept, modeling, and analysis," *IEEE Transactions on Smart Grid*, vol. 10, no. 3, pp. 2858–2870, 2019.

[2] O. Dranga, B. Buti, I. Nagy, and H. Funato, "Stability analysis of nonlinear power electronic systems utilizing periodicity and introducing auxiliary state vector," *IEEE Transactions on Circuits and Systems I: Regular Papers*, vol. 52, no. 1, pp. 168–178, 2005.

[3] Z. Shuai *et al.*, "Comparative Study of Short-Circuit Fault Characteristics for VSC-Based DC Distribution Networks with Different Distributed Generators," *IEEE Journal of Emerging and Selected Topics in Power Electronics*, vol. 7, no. 1, pp. 528–540, 2019.

[4] S. Cui and S. K. Sul, "A Comprehensive DC Short-Circuit Fault Ride Through Strategy of Hybrid Modular Multilevel Converters (MMCs) for Overhead Line Transmission," *IEEE Transactions on Power Electronics*, vol. 31, pp. 7780–7796, nov 2016.
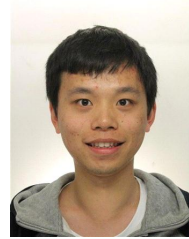
TABLE VIII
PARAMETERS OF TEST SYSTEMS

Parameter	Value (pu)	Parameter	Value (pu)
Test System 1			
$\underline{u}_{th}$	$1\angle0°$	$\underline{z}_{th}$	$0.01 + j0.1$
p_{ref}	0.5	u_{ref}	1
$\underline{z}_{vsc}$	$j0.1$	i_{vsc}^{max}	1
u_{vsc}^{max}	1.1	p_{vsc}^{max}	1
p_{vsc}^{min}	0	K_P^{fast}	1
K_I^{fast}	32	K_P^{slow}	20
K_I^{slow}	640		
Test System 2			
$\underline{u}_1$	$1\angle0°$	p_{ref2}	0.41
q_{ref2}	0.012	$\underline{z}_{vsc2}$	$j0.1$
i_{vsc2}^{max}	0.6	u_{vsc2}^{max}	1.1
p_{vsc2}^{max}	0.5	p_{vsc2}^{min}	0
p_{ref3}	0.21	q_{ref3}	-0.029
$\underline{z}_{vsc3}$	$j0.1$	i_{vsc3}^{max}	0.5
u_{vsc3}^{max}	1.1	p_{vsc3}^{max}	0.5
p_{vsc3}^{min}	0	p_5	0.56
q_5	0.21	$\underline{z}_{15}$	$0.01 + j0.068$
$\underline{z}_{16}$	$0.017 + j0.092$	$\underline{z}_{24}$	$0.0085+j0.058$
$\underline{z}_{25}$	$0.032 + j0.16$	$\underline{z}_{34}$	$0.012 + j0.10$
$\underline{z}_{36}$	$0.039 + j0.17$	$\underline{z}_{sc}$	$j0.01$
Test System 3			
$\underline{u}_1^{ref}$	$1.06\angle0°$	i_{vsc1}^{max}	1.5
θ_i^{ref}	$0°$	$\underline{z}_{vsc1}$	$j0.1$
u_{vsc1}^{max}	1.2	p_{vsc1}^{max}	1.5
p_{vsc1}^{min}	-1.5	p_{ref2}	0.4
q_{ref2}	0.5	$\underline{z}_{vsc2}$	$j0.1$
i_{vsc2}^{max}	0.75	u_{vsc2}^{max}	1.2
p_{vsc2}^{max}	0.75	p_{vsc2}^{min}	-0.75

[5] Y. Liu *et al.*, "Short-Circuit Current Estimation of Modular Multilevel Converter Using Discrete-Time Modeling," *IEEE Transactions on Power Electronics*, vol. 34, pp. 40–45, jan 2019.

[6] J. Beerten *et al.*, "Generalized Steady-State VSC MTDC Model for Sequential AC/DC Power Flow Algorithms," *IEEE Transactions on Power Systems*, vol. 27, pp. 821–829, may 2012.

[7] M. Aragüés-Peñalba *et al.*, "Optimal power flow tool for mixed high-voltage alternating current and high-voltage direct current systems for grid integration of large wind power plants," *IET Renewable Power Generation*, vol. 9, pp. 876–881, nov 2015.

[8] H. Ergun *et al.*, "Optimal Power Flow for AC-DC Grids: Formulation, Convex Relaxation, Linear Approximation, and Implementation," *IEEE Transactions on Power Systems*, vol. 34, pp. 2980–2990, jul 2019.

[9] F. D. Galiana, "Analytical Investigation of the Power Flow Equations.," in *Proceedings of the American Control Conference*, vol. 2, pp. 411–415, IEEE, 1983.

[10] A. Klos and J. Wojcicka, "Physical aspects of the nonuniqueness of load flow solutions," *International Journal of Electrical Power and Energy Systems*, vol. 13, no. 5, pp. 268–276, 1991.

[11] C. Wang *et al.*, "Explicit conditions on existence and uniqueness of load-flow solutions in distribution networks," *IEEE Transactions on Smart Grid*, vol. 9, no. 2, pp. 953–962, 2018.

[12] U. Sur and G. Sarkar, "A sufficient condition for multiple load flow solutions existence in three phase unbalanced active distribution networks," *IEEE Transactions on Circuits and Systems II: Express Briefs*, vol. 65, no. 6, pp. 784–788, 2018.

[13] D. Mehta *et al.*, "Numerical polynomial homotopy continuation method to locate all the power flow solutions," *IET Generation, Transmission and Distribution*, vol. 10, pp. 2972–2980, sep 2016.

[14] T. Van Cutsem and C. Vournas, *Voltage stability of electric power systems*. Springer US, 2008.

[15] D. M. Wolf and S. R. Sanders, "Multiparameter homotopy methods for finding dc operating points of nonlinear circuits," *IEEE Transactions on Circuits and Systems I: Fundamental Theory and Applications*, vol. 43, no. 10, pp. 824–838, 1996.

[16] Jaewook Lee and Hsiao-Dong Chiang, "Constructive homotopy methods for finding all or multiple dc operating points of nonlinear circuits and systems," *IEEE Transactions on Circuits and Systems I: Fundamental Theory and Applications*, vol. 48, no. 1, pp. 35–50, 2001.

[17] A. Ushida, Y. Yamagami, I. Kinouchi, Y. Nishio, and Y. Inoue, "An efficient algorithm for finding multiple dc solutions based on spice oriented newton homotopy method," in *ISCAS 2001. The 2001 IEEE International Symposium on Circuits and Systems (Cat. No.01CH37196)*, vol. 5, pp. 447–450 vol. 5, 2001.

[18] W. Ma and J. S. Thorp, "An efficient algorithm to locate all the load flow solutions," *IEEE Transactions on Power Systems*, vol. 8, no. 3, pp. 1077–1083, 1993.

[19] B. Lesieutre and D. Wu, "An efficient method to locate all the load flow solutions - Revisited," *2015 53rd Annual Allerton Conference on Communication, Control, and Computing, Allerton 2015*, vol. 1, pp. 381–388, 2016.

[20] B. Parkhideh and S. Bhattacharya, "Vector-controlled voltage-source-converter-based transmission under grid disturbances," *IEEE Transactions on Power Electronics*, vol. 28, no. 2, pp. 661–672, 2013.

[21] G. Wu *et al.*, "Analysis and design of vector control for VSC-HVDC connected to weak grids," *CSEE Journal of Power and Energy Systems*, vol. 3, pp. 115–124, jul 2017.

[22] J. Rocabert *et al.*, "Control of power converters in AC microgrids," *IEEE Transactions on Power Electronics*, vol. 27, no. 11, pp. 4734–4749, 2012.

[23] T. García-Sánchez *et al.*, "A review and discussion of the grid-code requirements for renewable energy sources in Spain," *Renewable Energy and Power Quality Journal*, vol. 1, no. 12, pp. 565–570, 2014.

[24] J. Verschelde, "Algorithm 795: PHCpack: A general-purpose solver for polynomial systems by homotopy continuation," *ACM Transactions on Mathematical Software*, vol. 25, no. 2, pp. 251–276, 1999.

[25] D. Mehta *et al.*, "Recent advances in computational methods for the power flow equations," *Proceedings of the American Control Conference*, vol. 2016-July, pp. 1753–1765, 2016.

[26] PSCAD, "IEEE 30 bus system technical note." https://www.pscad.com/uploads/knowledge_base/ieee_30_bus_technical_note.pdf, Dec. 2020.

Jie Song received the master degree in energy engineering from the School of Industrial Engineering of Barcelona (ETSEIB), Technical University of Catalonia (UPC), Barcelona, Spain and the master degree in electrical engineering from Royal Institute of Technology (KTH), Stockholm, Sweden, both in 2018. He is currently working towards a Ph.D. degree in electrical engineering at UPC and participating in CITCEA-UPC research group. His research interests include analysis of power systems with high penetration of power electronics.

Marc Cheah-Mane (S'14-M'18) received the degree in industrial engineering from the School of Industrial Engineering of Barcelona (ETSEIB), Universitat Politecnica de Catalunya (UPC), Barcelona, Spain, in 2013, and the PhD degree in electrical engineering from Cardiff University, Cardiff, the U.K. in 2017. From 2017 to 2020 he was a research associate in CITCEA-UPC, Barcelona, Spain. Since March 2020 he is a Serra Húnter Lecturer at the Electrical Engineering Department of UPC. His research interests include power systems with power electronics, high-voltage direct current systems, wind and photovoltaic generation.

Eduardo Prieto-Araujo (S'12-M'16) received the degree in industrial engineering from the School of Industrial Engineering of Barcelona (ETSEIB), Technical University of Catalonia (UPC), Barcelona, Spain, in 2011 and the Ph.D. degree in electrical engineering from the UPC in 2016. He joined CITCEA-UPC research group in 2010 and currently he is a Serra Húnter Lecturer with the Electrical Engineering Department, UPC. His main interests are renewable generation systems, control of power converters for HVDC applications, interaction analysis between converters, and power electronics dominated power systems.

Oriol Gomis-Bellmunt (S'05-M'07-SM'12-F'21) received the degree in industrial engineering from the School of Industrial Engineering of Barcelona (ETSEIB), Technical University of Catalonia (UPC), Barcelona, Spain, in 2001 and the Ph.D. degree in electrical engineering from the UPC in 2007. In 1999, he joined Engitrol S.L. where he worked as Project Engineer in the automation and control industry. Since 2004, he has been with the Electrical Engineering Department, UPC where he is a Professor and participates in the CITCEA-UPC Research Group. Since 2020, he is an ICREA Academia researcher. His research interests include the fields linked with electrical machines, power electronics, and renewable energy integration in power systems.